Constructing Heterostructure through Bidentate Coordination toward Operationally Stable Inverted Perovskite Solar Cells

Caiyi Zhang, Ting Guo, Luis K. Ono, Shuai Yuan, Tianhao Wu, Hengyuan Wang, Jiahao Zhang, Xiaomin Liu, Xiaomin Huo, Congyang Zhang, Chenfeng Ding, Tongtong Li, Yanbo Wang, Liyuan Han,* and Yabing Qi*

It has been reported that one of the influencing factors leading to stability issues in iodine-containing perovskite solar cells is the iodine loss from the perovskite layer. Herein, bidentate coordination is used with undercoordinated I^- of the perovskite surface to construct the stable perovskite-based heterostructure. This strong halogen bonding effectively inhibits interfacial migration of I^- into functional layers such as C_{60} and Ag. Moreover, passivation of the undercoordinated I^- suppresses the release of I_2 and further delays the formation of voids at the perovskite surface. The resulting inverted perovskite solar cell exhibits a power conversion efficiency of 22.59% and the unencapsulated device maintains 96.15% of its initial value after continuous operation for 500 h under illumination.

1. Introduction

Metal halide perovskite solar cells (PSCs) have been widely studied as a promising alternative photovoltaic technology due to their outstanding optoelectronic properties, such as high absorption coefficient, low exciton binding energy, and long carrier diffusion length.[1] During the past decade, the progressive increase in power conversion efficiency (PCE) from 3.8% to 25.7% has been witnessed.[2] Among the device structures, the inverted (p-i-n structure) PSCs, following the deposition sequence of hole transport layer (p), intrinsic perovskite layer (i), and electron transport layer (n), exhibit attractive features such as low-temperature processability, negligible hysteresis, promising stability due to the undoped charge transport layer and compatibility with tandem as well as flexible devices.[3] Recently, the performance of the inverted PSCs has seen substantial improvement mainly due to the development of the efficient perovskite-based heterojunction.[4] For example, Zhu et al. constructed the surface heterojunction by applying 3-(Aminomethyl) pyridine (3-APy) to react with the surface FA^+ of perovskite to reduce its surface potential fluctuations leading to n-type doping of the surface region, thus obtaining a PCE over 25%.[5] Xu et al. developed a porous insulator contact at the buried heterojunction to effectively reduce the nonradiative recombination without sacrificing the series resistance and achieved high Voc and FF with a certified PCE of 24.7%.[6] Moreover, researchers are also making significant progress in enhancing the PCE of perovskite modules via improving the uniformity of perovskite and other active layers.[7] In contrast, the instability of PSCs under operational conditions still poses a severe challenge to the commercialization of PSCs.

The weak bonding nature of perovskite makes the soft crystal lattice to degrade easily on the perovskite surface.[8] As a result, the perovskite components will diffuse and corrode the other functional layers including transport layer as well as electrodes.[9] The activation energy of I^- is small according to the theoretical calculations.[10] Consequently, I^- can easily migrate and generate I_2, especially on the surface due to half of the chemical bond compared with the bulk.[11] This is accelerated under operational conditions such as illumination and electric fields.[12] So far, the insertion of physical blocking layers is a promising strategy to inhibit I^- migration at the surface.[13] However, under long-term illumination and electric fields, iodine ions tend to diffuse through these physical blocking layers, thus promoting the degradation of the device. An additional instability factor arises from the generation of I_2 that induces the degradation of perovskite.[14] However, it is challenging to inhibit both the I_2 release and I^- invasion.

Halogen bonding has recently been employed in PSCs for interfacial toughening, crystallization manipulation, and trap

C. Zhang, Y. Wang, L. Han
State Key Laboratory of Metal Matrix Composites
Shanghai Jiao Tong University
Shanghai 200240, China
E-mail: han.liyuan@sjtu.edu.cn

C. Zhang, T. Guo, L. K. Ono, S. Yuan, T. Wu, H. Wang, J. Zhang, X. Liu, X. Huo, C. Zhang, C. Ding, T. Li, Y. B. Qi
Energy Materials and Surface Sciences Unit (EMSSU)
Okinawa Institute of Science and Technology Graduate University (OIST)
Okinawa 904-0495, Japan
E-mail: yabing.qi@oist.jp

The ORCID identification number(s) for the author(s) of this article can be found under https://doi.org/10.1002/solr.202300253.

passivation.[15] In addition, increasing the strength of halogen bonding can improve the performance and stability of devices.[16]

Here, 1,2-diiodotetrafluorobenzene (1,2-DITFB) is selected to form the bidentate coordination bond with undercoordinated I^- of the perovskite surface, thus obtaining strong halogen bonding according to the density functional theory (DFT) calculations and nuclear magnetic resonance (NMR) measurements. The stable perovskite/1,2-DITFB heterostructure is beneficial in inhibiting the I^- invasion into C_{60} and Ag via chemical bond (**Figure 1**a). Moreover, 1,2-DITFB could passivate the undercoordinated I^- on the perovskite surface, hence suppressing the release of I_2 and further delaying the formation of voids at the perovskite surface during operational conditions. As a result, 1,2-DITFB-based inverted PSCs exhibited a PCE of 22.59% and the unencapsulated devices maintained 96.15% of initial efficiency after 500 h aging under operational conditions at N_2.

2. Results and Discussion

Fluorinated analogs have been demonstrated to be effective for enhancing halogen bonding strength, such as the commonly used iodopenta-fluorobenzene (IPFB) and 1,4-DITFB molecules.[15b,g] This is ascribed to the positive electrostatic potentials (σ-hole) at the I atom side of the molecules, which could act as Lewis acid and coordinate with the I^- (Lewis base) from

perovskite (Figure 1b). However, IPFB and 1,4-DITFB tend to adsorb at the perovskite surface via a monodentate coordination (Figure 1a), which can be easily broken owing to the low binding strength.[17] To solve this issue without sacrificing the halogen bonding, 1,2-DITFB was selected to form the bidentate coordination with perovskite. To confirm this, we used the DFT calculations to study the adsorption mode for the 1,2-DITFB on an I-terminated (001) perovskite surface.[15e,f] The energy for the bidentate coordination (-251.15 eV) is lower compared with the monodentate coordination (−250.65 eV), indicating that 1,2-DITFB is more likely to be absorbed on the surface of perovskite via the bidentate mode (Figure S1, Supporting Information). After the structure optimization of the perovskite/designated molecules (Figure S2, Supporting Information), there is obvious charge density accumulation between σ-hole from the selected molecules and I^- from perovskite, which confirms the presence of halogen–halogen bonds in those complexes (Figure 1a).[16a] However, there are two I atoms involved in the formation of halogen bonding in the 1,2-DITFB case, while only one I atom is involved in the formation of halogen bonding in both the IPFB and 1,4-DITFB case (Figure 1a). This also indicates that 1,2-DITFB forms the bidentate coordination with perovskite in contrast with the monodentate coordination in that of IPFB and 1,4-DITFB. The side and top view for bidentate coordination in 1,2-DITFB and perovskite are displayed in Figure S3, Supporting Information. To explore the effect of the bidentate
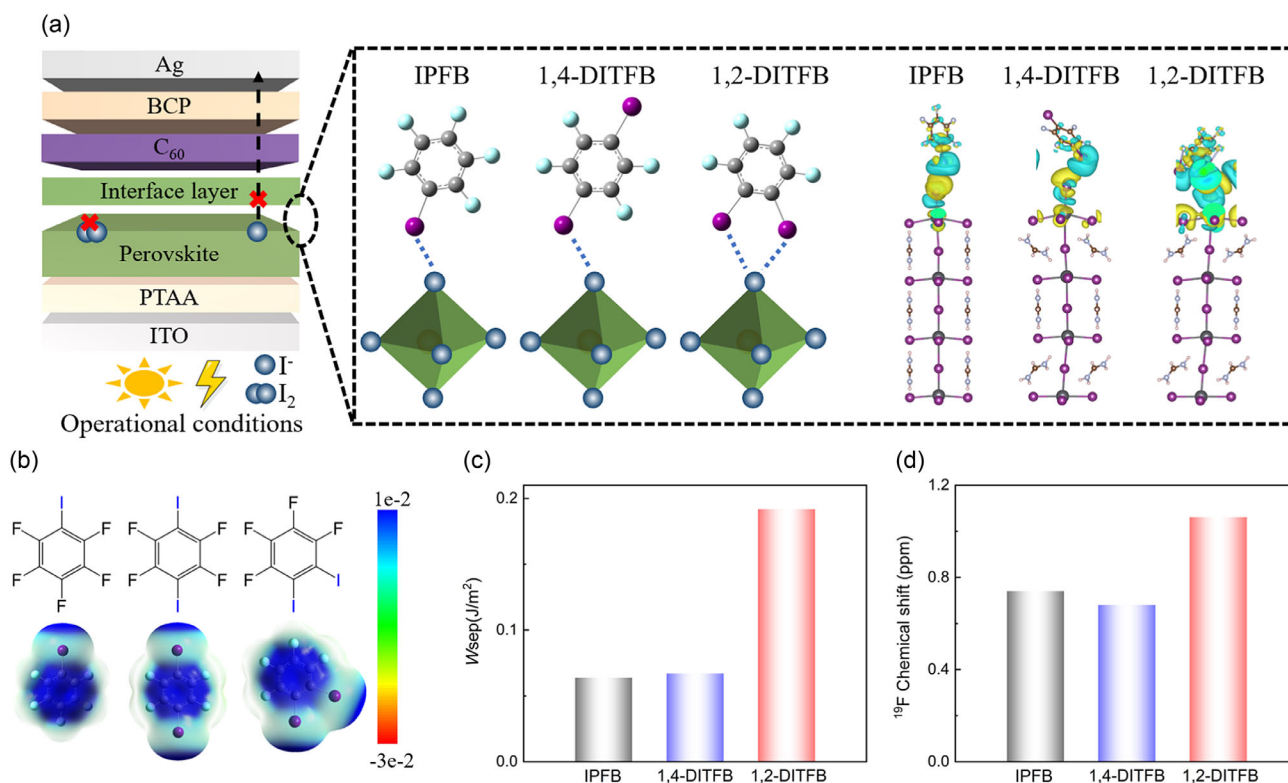

Figure 1. a) Schematic of the device structure, the coordination mode between the perovskite and selected molecules (IPFB, 1,4-DITFB, and 1,2-DITFB), and the corresponding charge transfer density difference plots from DFT calculations. The contour value for the isodensity plot is 0.0002. The positive charge density regions are highlighted in yellow, and the negative ones in blue. b) The electrostatic potentials of the selected molecules. The color bar from red to blue represents the increase in electropositivity. c) The absolute work of separation (Wsep) values for the selected molecules and perovskite (I-terminated) surface from the DFT calculation. d) Change of ^{19}F NMR chemical shift for selected molecules after the addition of PbI_2 and FAI.

coordination on the adhesion strength, DFT calculations were employed to obtain the work of separation (Wsep).[15f,18] The absolute Wsep value of perovskite with 1,2-DITFB (0.192 J m^{-2}) was about three times that with IPFB (0.0638 J m^{-2}) or 1,4-DITFB (0.067 J m^{-2}) (Figure 1c), which could be ascribed to the bidentate coordination in the 1,2-DITFB case. To further illustrate the effect of the bidentate mode on the strength of the halogen bonding, NMR measurements were employed to characterize the interaction between IPFB, 1,4-DITFB, 1,2-DITFB, and the perovskite. To indicate the halogen bonding, we first only mix the PbI_2 with selected molecules. Compared with the pristine molecules, the chemical shifts of F in 1,2-DITFB (0.561 ppm) mixed with the PbI_2 are much larger than that of the IPFB (0.408 ppm) or 1,4-DITFB (0.354 ppm) mixed with the PbI_2 (Figure S4, Supporting Information), which is related to the bidentate mode in 1,2-DITFB and is consistent with the DFT calculations. [16a,21b] To further confirm the halogen bonding between the molecules and perovskite, we further add FAI into the mixture of PbI_2 and molecules. Similarly, the chemical shifts of the F in 1,2-DITFB (1.062 ppm) mixed with the FAI and PbI_2 are much larger than that of the IPFB (0.741 ppm) or 1,4-DITFB (0.680 ppm) mixed with the FAI and PbI_2 (Figure 1d and S4, Supporting Information).

Due to the coordination with I$^-$ from perovskite and selected molecules, this halogen bonding is expected to passivate the undercoordinated I$^-$ traps and suppress the interfacial migration of I$^-$ via chemical bond. Furthermore, 1,2-DITFB was employed at the surface of perovskite to investigate the effect of bidentate coordination on the stability and efficiency of the surface heterojunction and the devices. On the basis of the scanning electron microscopy (SEM), X-Ray diffraction (XRD), and ultraviolet–visible (UV–vis) absorption spectroscopy results (Figure S5–S7, Supporting Information), the additional molecular layer (IPFB, 1,4-DITFB, or 1,2-DITFB) spin-coated on the perovskite sample only leads to negligible change to the morphology, crystallinity, and bandgap of the perovskite film.

The effect of bidentate coordination on I$^-$ migration in the solar cell device under operational conditions is investigated. To directly detect I$^-$ migration, the Ag electrodes of the device were peeled off by carbon tape (**Figure 2**a).[19] As a result, the surface of perovskite/C_{60} and the Ag electrodes could be obtained (Figure S8, Supporting Information). Obvious I signals could be detected in the Ag electrodes for the control device after operational aging, indicating I$^-$ diffusion toward the Ag cathode (Figure 2b). In contrast, the I signal in the Ag electrodes from the 1,2-DITFB device was the smallest compared with the control, IPFB, and 1,4-DITFB device, implying that 1,2-DITFB suppresses I$^-$ diffusion effectively. Moreover, the integrated area ratio of aged control and aged 1,2-DITFB on I 3d$_{5/2}$ peak was found to be 6.39. In addition, a similar phenomenon was also observed at the surface of perovskite/C_{60} (Figure S9, Supporting Information). To further verify this point, the
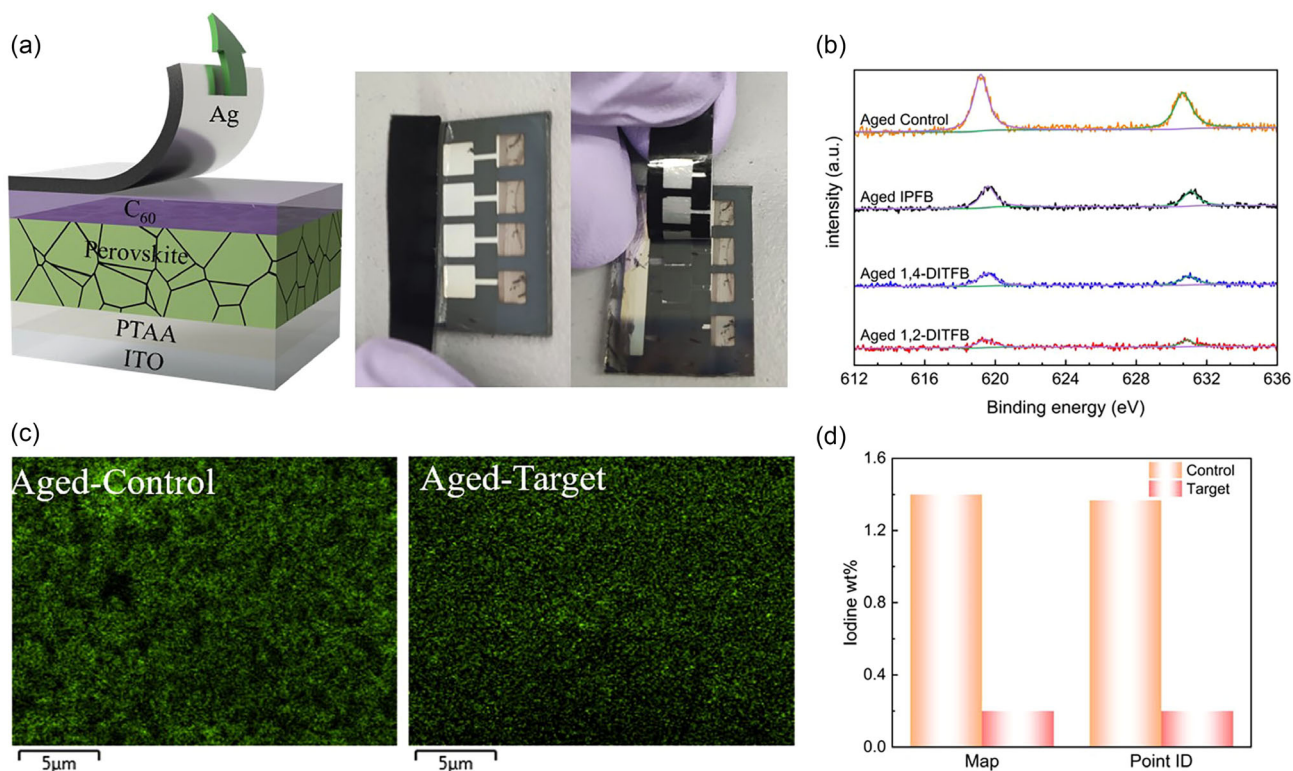

Figure 2. a) Schematic diagrams of the peeling-off process of the Ag electrodes from the devices and corresponding photos. b) XPS spectra of the I 3d core level of the aged Ag electrodes surface from the device without treatment (orange), with IPFB (black), with 1,4-DITFB (blue), and 1,2-DITFB (red). c) EDX mapping and d) the corresponding weight percentage of iodine in the aged Ag electrodes surface from the device without treatment (orange) and with 1,2-DITFB (red).

exposed Ag electrodes from the device without and with 1,2-DITFB are measured with SEM-EDX. From the mapping and point ID spectrum, the I weight ratio (wt%) of the exposed Ag electrodes in the fresh device is 0.0% (Figure S10 and S11, Supporting Information). After aging under operational conditions, the exposed Ag electrodes in the control device show a stronger I signal than that of the 1,2-DITFB device (Figure 2c). In addition, the corresponding mapping spectrum in the exposed Ag electrodes in the control device (1.4%) exhibits a higher I content compared with the 1,2-DITFB treated device (0.2%) (Figure S12, Supporting Information). The point ID profile in the exposed Ag electrodes showed a similar trend (Figure 2d and S13, Supporting Information). These results indicate that the stronger halogen bonding in 1,2-DITFB via bidentate coordination suppresses more effectively the I invasion into other functional layers.

We also conducted Kelvin probe force microscopy (KPFM) to investigate the electrical properties of the exposed C_{60} layer. The contact potential difference (CPD) of aged perovskite/1,2-DITFB/C_{60} was similar to that of the fresh sample, but the CPD of the aged perovskite/C_{60} is 98 mV lower than that of the fresh sample (**Figure 3a–c**), where the corresponding AFM image is shown in Figure S14, Supporting Information. In addition, the CPD distribution of the aged samples is analyzed in Figure S15, Supporting Information; the aged sample with 1,2-DITFB showed a narrower distribution compared with the aged sample without the 1,2-DITFB treatment, indicating the homogeneous surface of C_{60} in the device with the 1,2-DITFB treatment. In addition, previous works show that when migrated I contacts Ag electrode, AgI (semiconductor) is formed leading to lower conductivity, which could induce energy level mismatch and decrease the device performance.[9c,20] Besides eroding the other functional layer (C_{60}, Ag), the undercoordinated I^- is likely to degrade the perovskite layer via the generation of I_2.[9b] During the operation, the undercoordinated I^- on the surface of perovskite captures a hole to form a neutral I atom. Furthermore, two I atoms diffuse and combine to generate I_2.[14c] To verify this, we adopted UV–vis spectroscopy to characterize the formation of I_2 in the control and 1,2-DITFB treated films. An absorption band at 500 nm corresponds to the complex between toluene and I_2.[9b,14c] After exposing the toluene-submersed films to light for 48 h, we observed a faster release of I_2 from the control film compared with the sample with the 1,2-DITFB treatment in Figure 3d.

Owing to the passivation of the undercoordinated I^- on the surface of perovskite, the suppression of I_2 in 1,2-DITFB could further inhibit the formation of voids on the surface of perovskite (Figure 3e,f), consistent with previous reports.[21] These voids hinder the extraction of charge carriers and act as a reservoir for I_2 to further trigger the degradation of the perovskite.[14a,b,d,22] To confirm this, we conducted photoluminescence (PL) to characterize the nonradiative recombination of perovskite. The fresh film treated with 1,2-DITFB showed stronger PL intensity than that of the control film, indicating less nonradiative recombination and a lower concentration of trap states (Figure S16, Supporting Information). This observation is consistent with the lower current leakage in the device treated with 1,2-DITFB (3.051×10^{-9} mA cm^{-2}) than the control device
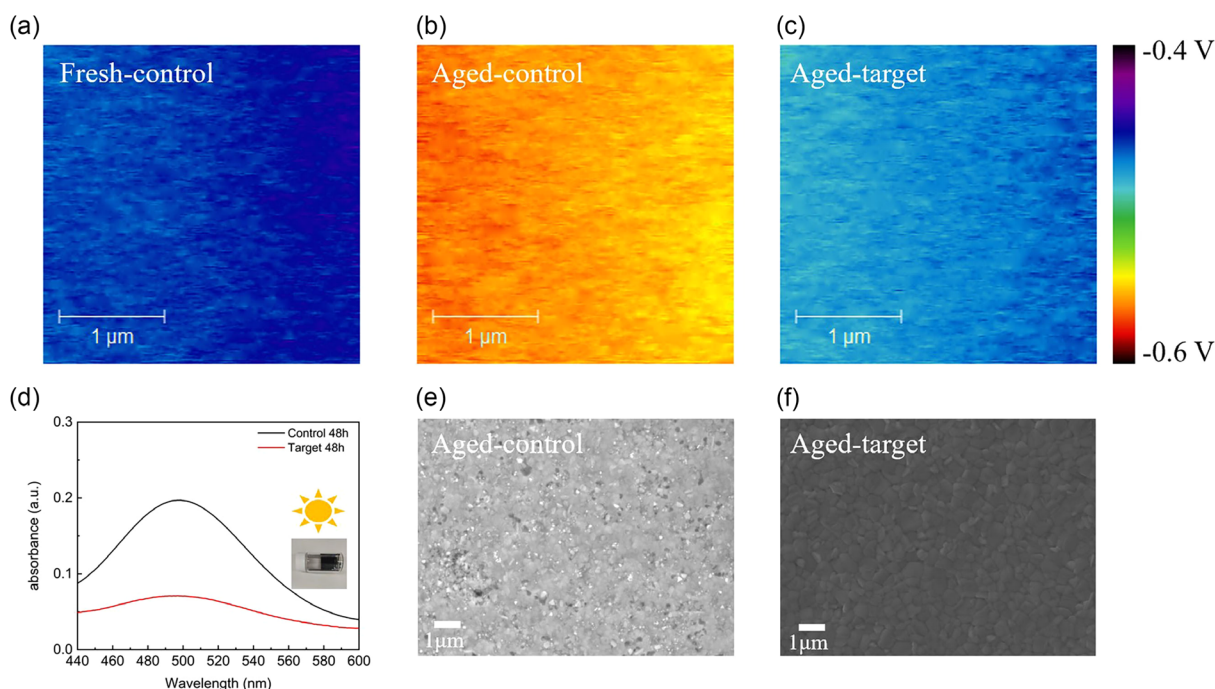

Figure 3. Surface potential mapping of the perovskite/C_{60} film from the device without treatment a) before aging and b) after aging, and c) with 1,2-DITFB after aging. d) UV–vis absorbance spectra for the toluene solution collected from the control and 1,2-DITFB treated vials after light soaking. The band at 500 nm corresponds to the complex (toluene reacted with I_2). The corresponding morphology of the perovskite/C_{60} from the device e) without treatment and f) with 1,2-DITFB after aging.

$(1.221 \times 10^{-8}\,\text{mA cm}^{-2})$ in dark J–V measurements (Figure S17, Supporting Information). After aging, the PL intensity barely changes for the film treated with 1,2-DITFB, whereas the control film shows a significant decrease and the recombination becomes severer due to voids. On the basis of these results, we can conclude that a stabilized heterostructure of perovskite/1,2-DITFB is formed.

We fabricated PSCs with and without a perovskite/1,2-DITFB heterostructure. The cross-sectional SEM images of these PSCs are shown in **Figure 4**a (the PSC with a perovskite/1,2-DITFB heterostructure) and Figure S18, Supporting Information (the control PSC without a perovskite/1,2-DITFB heterostructure). The current density–voltage (J–V) curves of cells with different heterostructures are presented in Figure 4b. The target device exhibited a PCE of 22.59% empowered by a high open-circuit voltage (V_{oc}) of 1.17 V, a short-circuit current density (J_{sc}) of 24.09 mA cm^{-2}, and a fill factor (FF) of 79.97%, whereas the control device showed a PCE of 21.50% with a V_{oc} of 1.5 V, a J_{sc} of 24.00 mA cm^{-2}, and a FF of 78.02%. The improved V_{oc} and FF are ascribed to the undercoordinated I$^-$ passivation. Both control and target devices exhibited high external quantum efficiency values (Figure 4c), consistent with their similar J_{sc} from J–V curves. Operational stability measurements are important for PSCs because light illumination and a number of other external factors can accelerate the degradation of the soft perovskite interface. The home-designed test system with heater and thermocouple is employed to conduct accelerated aging, according to the International Summit on Organic Photovoltaic Stability (ISOS)

protocols (Figure S19, Supporting Information).[13a] A bias close to the voltage at the maximum power point (MPP) was applied to the corresponding PSCs in the N$_2$-filled chamber with 5% relative humidity for tracking the power output. The device temperature (25 °C) was monitored using a thermocouple during the operation. Only 78.18% of the initial PCE was retained in control PSCs after tracking for 208 h, while PSCs with 1,2-DITFB retained 96.15% of their initial PCE under operational conditions for 500 h (Figure 4d). The enhanced long-term operational stability is assigned to the stabilized heterostructure via bidentate coordination in perovskite/1,2-DITFB, which inhibits the I$^-$ interfacial migration and I$_2$ release.

3. Conclusion

In summary, 1,2-DITFB molecules based on IPFB and 1,4-DITFB were found to form a stronger halogen bonding with the undercoordinated I$^-$ at the surface of the perovskite film owing to the bidentate coordination. As a result, the constructed stable heterostructure of perovskite/1,2-DITFB is proven to more effectively suppress the I$^-$ migration compared with that of perovskite/IPFB or perovskite/1,4-DITFB. Therefore, the pristine electrical properties of C$_{60}$ and Ag electrodes could be maintained after operational aging. Moreover, this halogen bonding reduces the undercoordinated I$^-$ defects of the perovskite surface, thus suppressing the nonradiative recombination and I$_2$ release. The reduced I$_2$ in perovskite/1,2-DITFB
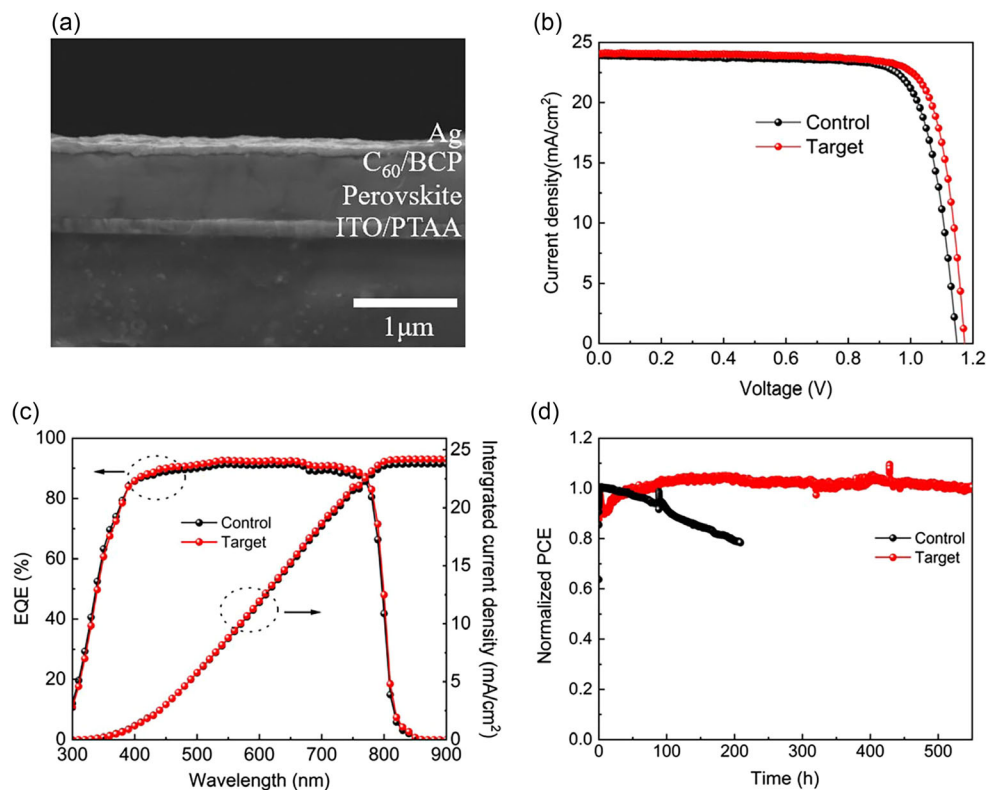

Figure 4. a) Cross-sectional SEM image of the device with 1,2-DITFB. b) J–V curves and c) EQE curves of the control and 1,2-DITFB devices. d) Operational stability of the unencapsulated PSCs at N$_2$ measured under room temperature (25 °C) at a fixed bias.

heterostructure inhibits the formation of voids when the devices are under operational conditions. Therefore, the champion device based on 1,2-DITFB exhibited a PCE of 22.59% and the corresponding unencapsulated device maintained 96.15% of their initial PCE after 500 h continuous operation aging under the illumination. This study provides a new way to regulate the strength of halogen bonding between perovskite and molecules via bidentate mode.

Supporting Information

Supporting Information is available from the Wiley Online Library or from the author.

Conflict of Interest

The authors declare no conflict of interest.

Author Contributions

Y.B.Q. and L.H. supervised this research project. Caiyi Zhang conceived the idea. Caiyi Zhang and Y.B.Q. designed the experiments, performed the data analysis, and wrote the draft manuscript. Caiyi Zhang, L.H., Y.B.Q., S.Y., and Y.W. participated in the discussion about the experimental details. Caiyi Zhang conducted the solar cell fabrication and performed the characterizations. T.G. helped with the DFT calculation. L.K.O. provided support for the measurements including XPS, dark J–V, UV–vis, and stability. T.W. and H.W. provided support for the KPFM measurements. J.Z., X.L., and X.H. provided support for the sample preparation. Congyang Zhang and C.D. provided support for the NMR measurements. S.Y. provided support for the analysis of the NMR results. T.L. provided support for the SEM measurements. All authors contributed to revising the article.

Data Availability Statement

The data that support the findings of this study are available in the supplementary material of this article.

[1] a) M. A. Green, A. Ho-Baillie, H. J. Snaith, *Nat. Photonics* **2014**, *8*, 506; b) S. D. Stranks, G. E. Eperon, G. Grancini, C. Menelaou, M. J. P. Alcocer, T. Leijtens, L. M. Herz, A. Petrozza, H. J. Snaith, *Science* **2013**, *342*, 341; c) A. Miyata, A. Mitioglu, P. Plochocka, O. Portugall, J. T. W. Wang, S. D. Stranks, H. J. Snaith, R. J. Nicholas, *Nat. Phys.* **2015**, *11*, 582.

[2] a) A. Kojima, K. Teshima, Y. Shirai, T. Miyasaka, *J. Am. Chem. Soc.* **2009**, *131*, 6050; b) Best Research-Cell Efficiency Chart | Photovoltaic Research | NREL https://www.nrel.gov/pv/cell-efficiency.html (accessed: March 2023).

[3] a) F. Ma, Y. Zhao, J. Li, X. Zhang, H. Gu, J. You, *J. Energy Chem.* **2021**, *52*, 393; b) C. Chen, J. Liang, J. Zhang, X. Liu, X. Yin, H. Cui, H. Wang, C. Wang, Z. Li, J. Gong, Q. Lin, W. Ke, C. Tao, B. Da, Z. Ding, X. Xiao, G. Fang, *Nano Energy* **2021**, *90*, 106608; c) A. Y. Alsalloum, B. Turedi, K. Almasabi, X. Zheng, R. Naphade, S. D. Stranks, O. F. Mohammed, O. M. Bakr, *Energy Environ. Sci.* **2021**, *14*, 2263; d) S. Yang, J. Dai, Z. Yu, Y. Shao, Y. Zhou, X. Xiao, X. C. Zeng, J. Huang, *J. Am. Chem. Soc.* **2019**, *141*, 5781; e) W. Chen, Y. Zhou, G. Chen, Y. Wu, B. Tu, F.-Z. Liu, L. Huang, A. M. C. Ng, A. B. Djurišić, Z. He, *Adv. Energy Mater.* **2019**, *9*, 1803872.

[4] a) C. Li, X. Wang, E. Bi, F. Jiang, S. M. Park, Y. Li, L. Chen, Z. Wang, L. Zeng, H. Chen, Y. Liu, C. R. Grice, A. Abudulimu, J. Chung, Y. Xian, T. Zhu, H. Lai, B. Chen, R. J. Ellingson, F. Fu, D. S. Ginger, Z. Song, E. H. Sargent, Y. Yan, *Science* **2023**, *379*, 690; b) P. Chen, Y. Xiao, L. Li, L. Zhao, M. Yu, S. Li, J. Hu, B. Liu, Y. Yang, D. Luo, C.-H. Hou, X. Guo, J.-J. Shyue, Z.-H. Lu, Q. Gong, H. J. Snaith, R. Zhu, *Adv. Mater.* **2023**, *35*, 2 206345; c) Z. Li, B. Li, X. Wu, S. A. Sheppard, S. Zhang, D. Gao, N. J. Long, Z. Zhu, *Science* **2022**, *376*, 416; d) X. Zheng, Y. Hou, C. Bao, J. Yin, F. Yuan, Z. Huang, K. Song, J. Liu, J. Troughton, N. Gasparini, C. Zhou, Y. Lin, D.-J. Xue, B. Chen, A. K. Johnston, N. Wei, M. N. Hedhili, M. Wei, A. Y. Alsalloum, P. Maity, B. Turedi, C. Yang, D. Baran, T. D. Anthopoulos, Y. Han, Z.-H. Lu, O. F. Mohammed, F. Gao, E. H. Sargent, O. M. Bakr, *Nat. Energy* **2020**, *5*, 131; e) S. Wu, J. Zhang, Z. Li, D. Liu, M. Qin, S. H. Cheung, X. Lu, D. Lei, S. K. So, Z. Zhu, A. K. Y. Jen, *Joule* **2020**, *4*, 1248; f) F. Li, X. Deng, F. Qi, Z. Li, D. Liu, D. Shen, M. Qin, S. Wu, F. Lin, S.-H. Jang, J. Zhang, X. Lu, D. Lei, C.-S. Lee, Z. Zhu, A. K. Y. Jen, *J. Am. Chem. Soc.* **2020**, *142*, 20134; g) W.-Q. Wu, Z. Yang, P. N. Rudd, Y. Shao, X. Dai, H. Wei, J. Zhao, Y. Fang, Q. Wang, Y. Liu, Y. Deng, X. Xiao, Y. Feng, J. Huang, Science Advances **2019**, 5, eaav8925; h) D. Y. Luo, W. Q. Yang, Z. P. Wang, A. Sadhanala, Q. Hu, R. Su, R. Shivanna, G. F. Trindade, J. F. Watts, Z. J. Xu, T. H. Liu, K. Chen, F. J. Ye, P. Wu, L. C. Zhao, J. Wu, Y. G. Tu, Y. F. Zhang, X. Y. Yang, W. Zhang, R. H. Friend, Q. H. Gong, H. J. Snaith, R. Zhu, *Science* **2018**, *360*, 1442; i) S. Zhang, F. Ye, X. Wang, R. Chen, H. Zhang, L. Zhan, X. Jiang, Y. Li, X. Ji, S. Liu, M. Yu, F. Yu, Y. Zhang, R. Wu, Z. Liu, Z. Ning, D. Neher, L. Han, Y. Lin, H. Tian, W. Chen, M. Stolterfoht, L. Zhang, W.-H. Zhu, Y. Wu, *Science* **2023**, *380*, 404; j) R. Azmi, E. Ugur, A. Seitkhan, F. Aljamaan, A. S. Subbiah, J. Liu, G. T. Harrison, M. I. Nugraha, M. K. Eswaran, M. Babics, Y. Chen, F. Xu, T. G. Allen, A. U. Rehman, C.-L. Wang, T. D. Anthopoulos, U. Schwingenschlögl, M. De Bastiani, E. Aydin, S. De Wolf, *Science* **2022**, *376*, 73.

[5] Q. Jiang, J. Tong, Y. Xian, R. A. Kerner, S. P. Dunfield, C. Xiao, R. A. Scheidt, D. Kuciauskas, X. Wang, M. P. Hautzinger, R. Tirawat, M. C. Beard, D. P. Fenning, J. J. Berry, B. W. Larson, Y. Yan, K. Zhu, *Nature* **2022**, *611*, 278.

[6] W. Peng, K. Mao, F. Cai, H. Meng, Z. Zhu, T. Li, S. Yuan, Z. Xu, X. Feng, J. Xu, M. D. McGehee, J. Xu, *Science* **2023**, *379*, 683.

[7] a) T. Bu, L. K. Ono, J. Li, J. Su, G. Tong, W. Zhang, Y. Liu, J. Zhang, J. Chang, S. Kazaoui, F. Huang, Y.-B. Cheng, Y. B. Qi, *Nat. Energy*

2022, *7*, 528; b) Z. Yang, W. Zhang, S. Wu, H. Zhu, Z. Liu, Z. Liu, Z. Jiang, R. Chen, J. Zhou, Q. Lu, Z. Xiao, L. Shi, H. Chen, L. K. Ono, S. Zhang, Y. Zhang, Y. B. Qi, L. Han, W. Chen, *Sci. Adv.* **2021**, *7*, eabg3749; c) T. Bu, J. Li, H. Li, C. Tian, J. Su, G. Tong, L. K. Ono, C. Wang, Z. Lin, N. Chai, X.-L. Zhang, J. Chang, J. Lu, J. Zhong, W. Huang, Y. B. Qi, Y.-B. Cheng, F. Huang, *Science* **2021**, *372*, 1327; d) S. Chen, X. Dai, S. Xu, H. Jiao, L. Zhao, J. Huang, *Science* **2021**, *373*, 902; e) N. Li, J. Liu, C. Li, Y. Li, J. Jia, Y. Wu, H. Yu, B. Yuan, B. Cao, *ACS Sustain. Chem. Eng.* **2020**, *8*, 7020; f) N. Li, F. Xu, Z. Qiu, J. Liu, X. Wan, X. Zhu, H. Yu, C. Li, Y. Liu, B. Cao, *J. Power Sources* **2019**, *426*, 188.

[8] a) Y. Wang, T. Wu, J. Barbaud, W. Kong, D. Cui, H. Chen, X. Yang, L. Han, *Science* **2019**, *365*, 687; b) X. Li, W. Zhang, X. Guo, C. Lu, J. Wei, J. Fang, *Science* **2022**, *375*, 434.

[9] a) E. B. Bi, H. Chen, F. X. Xie, Y. Z. Wu, W. Chen, Y. J. Su, A. Islam, M. Gratzel, X. D. Yang, L. Y. Han, *Nat. Commun.* **2017**, *8*, 7; b) A. Krishna, H. Zhang, Z. Zhou, T. Gallet, M. Dankl, O. Ouellette, F. T. Eickemeyer, F. Fu, S. Sanchez, M. Mensi, S. M. Zakeeruddin, U. Rothlisberger, G. N. Manjunatha Reddy, A. Redinger, M. Grätzel, A. Hagfeldt, *Energy Environ. Sci.* **2021**, *14*, 5552; c) Y. Kato, L. K. Ono, M. V. Lee, S. H. Wang, S. R. Raga, Y. B. Qi, *Adv. Mater. Interfaces* **2015**, *2*, 6.

[10] a) C. Eames, J. M. Frost, P. R. F. Barnes, B. C. O'Regan, A. Walsh, M. S. Islam, *Nat. Commun.* **2015**, *6*, 7497; b) J. M. Azpiroz, E. Mosconi, J. Bisquert, F. De Angelis, *Energy Environ. Sci.* **2015**, *8*, 2118.

[11] W. K. Zhu, S. R. Wang, X. Zhang, A. L. Wang, C. Wu, F. Hao, *Small* **2022**, *18*, 2105783.

[12] a) P. V. Kamat, M. Kuno, *Acc. Chem. Res.* **2021**, *54*, 520; b) D. Lin, T. Shi, H. Xie, F. Wan, X. Ren, K. Liu, Y. Zhao, L. Ke, Y. Lin, Y. Gao, X. Xu, W. Xie, P. Liu, Y. Yuan, *Adv. Energy Mater.* **2021**, *11*, 2002552; c) H. C. Zai, Y. Ma, Q. Chen, H. P. Zhou, *J. Energy Chem.* **2021**, *63*, 528.

[13] a) T. Wu, L. K. Ono, R. Yoshioka, C. Ding, C. Zhang, S. Mariotti, J. Zhang, K. Mitrofanov, X. Liu, H. Segawa, R. Kabe, L. Han, Y. B. Qi, *Energy Environ. Sci.* **2022**, *15*, 4612.; b) H. P. Zeng, L. Li, F. X. Liu, M. Li, S. J. Zhang, X. Zheng, L. Luo, S. You, Y. Zhao, R. Guo, Z. M. Gong, R. Huang, Z. Li, T. Wang, Y. Cui, Y. G. Rong, X. Li, *Adv. Energy Mater.* **2022**, *12*, 2102820; c) J. Xu, J. Xi, H. Dong, N. Ahn, Z. L. Zhu, J. B. Chen, P. Z. Li, X. Y. Zhu, J. F. Dai, Z. Y. Hu, B. Jiao, X. Hou, J. R. Li, Z. X. Wu, *Nano Energy* **2021**, *88*, 106286; d) Y. Ma, Y. Cheng, X. Xu, M. Li, C. Zhang, S. H. Cheung, Z. Zeng, D. Shen, Y.-M. Xie, K. L. Chiu, F. Lin, S. K. So, C.-S. Lee, S.-W. Tsang, *Adv. Funct. Mater.* **2021**, *31*, 2006802; e) Q. Cao, Y. Li, H. Zhang, J. Yang, J. Han, T. Xu, S. Wang, Z. Wang, B. Gao, J. Zhao, X. Li, X. Ma, S. M. Zakeeruddin, W. E. I. Sha, X. Li, M. Graetzel, *Sci. Adv.* **2021**, *7*, eabg0633.

[14] a) S. Wang, Y. Jiang, Emilio J. Juarez-Perez, *Nat. Energy* **2016**, *2*, 16195; b) S. Chen, X. Xiao, H. Gu, J. Huang, *Sci. Adv.* **2021**, *7*, eabe8130; c) Y.-H. Lin, N. Sakai, P. Da, J. Wu, H. C. Sansom, A. J. Ramadan, S. Mahesh, J. Liu, R. D. J. Oliver, J. Lim, L. Aspitarte, K. Sharma, P. K. Madhu, A. B. Morales-Vilches, P. K. Nayak, S. Bai, F. Gao, C. R. M. Grovenor, M. B. Johnston, J. G. Labram, J. R. Durrant, J. M. Ball, B. Wenger, B. Stannowski, H. J. Snaith, *Science* **2020**, *369*, 96; d) S. G. Motti, D. Meggiolaro, A. J. Barker, E. Mosconi, C. A. R. Perini, J. M. Ball, M. Gandini, M. Kim, F. De Angelis, A. Petrozza, *Nat. Photonics* **2019**, *13*, 532.

[15] a) E. Ochoa-Martinez, J. V. Milić, *Nat. Energy* **2021**, *6*, 858; b) M. A. Ruiz-Preciado, D. J. Kubicki, A. Hofstetter, L. McGovern, M. H. Futscher, A. Ummadisingu, R. Gershoni-Poranne, S. M. Zakeeruddin, B. Ehrler, L. Emsley, J. V. Milić, M. Grätzel, *J. Am. Chem. Soc.* **2020**, *142*, 1645; c) S. Bi, H. Wang, J. Zhou, S. You, Y. Zhang, X. Shi, Z. Tang, H. Zhou, *J. Mater. Chem. A* **2019**, *7*, 6840; d) L. Canil, T. Cramer, B. Fraboni, D. Ricciarelli, D. Meggiolaro, A. Singh, M. Liu, M. Rusu, C. M. Wolff, N. Phung, Q. Wang, D. Neher, T. Unold, P. Vivo, A. Gagliardi, F. De Angelis, A. Abate, *Energy Environ. Sci.* **2021**, *14*, 1429; e) C. M. Wolff, L. Canil, C. Rehermann, N. Ngoc Linh, F. Zu, M. Ralaiarisoa, P. Caprioglio, L. Fiedler, M. Stolterfoht, S. Kogikoski, I. Bald, N. Koch, E. L. Unger, T. Dittrich, A. Abate, D. Neher, *ACS Nano* **2020**, *14*, 1445; f) Z. Dai, S. K. Yadavalli, M. Chen, A. Abbaspourtamijani, Y. Qi, N. P. Padture, *Science* **2021**, *372*, 618; g) A. Abate, M. Saliba, D. J. Hollman, S. D. Stranks, K. Wojciechowski, R. Avolio, G. Grancini, A. Petrozza, H. J. Snaith, *Nano Lett.* **2014**, *14*, 3247; h) P. Metrangolo, L. Canil, A. Abate, G. Terraneo, G. Cavallo, *Angew. Chem. Int. Ed. Engl.* **2022**, *61*, 202114793; i) M. L. Ball, J. V. Milić, Y.-L. Loo, *Chem. Mat.* **2022**, *34*, 2495.

[16] a) X. Fu, T. He, S. Zhang, X. Lei, Y. Jiang, D. Wang, P. Sun, D. Zhao, H.-Y. Hsu, X. Li, M. Wang, M. Yuan, *Chem* **2021**, *7*, 3131; b) D. Zhang, P. Jiang, D. Li, S. Li, J. Qi, X. Wang, Y. Hu, Y. Rong, A. Mei, H. Han, *Sol. RRL* **2022**, *6*, 2100851.

[17] a) E. Li, C. Liu, H. Lin, X. Xu, S. Liu, S. Zhang, M. Yu, X.-M. Cao, Y. Wu, W.-H. Zhu, *Adv. Funct. Mater.* **2021**, *31*, 2103847; b) H. Zhang, Y. Wu, C. Shen, E. Li, C. Yan, W. Zhang, H. Tian, L. Han, W. H. Zhu, *Adv. Energy Mater.* **2019**, *9*, 1803573.

[18] Y. Qi, L. G. Hector, *Phys. Rev. B* **2004**, *69*, 235401.

[19] J. Y. Ning, Y. N. Zhu, Z. Hu, Y. H. Shi, M. Ali, J. P. He, Y. W. He, F. Yan, S. H. Yang, J. S. Miao, H. Meng, *Adv. Funct. Mater.* **2020**, *30*, 2000837.

[20] J. Li, Q. Dong, N. Li, L. Wang, *Adv. Energy Mater.* **2017**, *7*, 1602922.

[21] a) F. Fu, S. Pisoni, Q. Jeangros, J. Sastre-Pellicer, M. Kawecki, A. Paracchino, T. Moser, J. Werner, C. Andres, L. Duchene, P. Fiala, M. Rawlence, S. Nicolay, C. Ballif, A. N. Tiwari, S. Buecheler, *Energy Environ. Sci.* **2019**, *12*, 3074; b) C. Zhang, X. Shen, M. Chen, Y. Zhao, X. Lin, Z. Qin, Y. Wang, L. Han, *Adv. Energy Mater.* **2023**, *13*, 2203250.

[22] N. Aristidou, I. Sanchez-Molina, T. Chotchuangchutchaval, M. Brown, L. Martinez, T. Rath, S. A. Haque, *Angew. Chem. Int. Ed.* **2015**, *54*, 8208.